

A correlation between drag and an integral property of the wake

T. S. Morton*

Abstract

An integral quantity is presented which appears to relate the wake of a body in nominally two-dimensional flow to its drag, without the use of viscosity. It is defined in a region of fluid as the ratio of the kinetic energy to the vorticity in the fluid boundary and, for the special case of laminar flow, is proportional to the angular momentum of the fluid. A relation involving the new quantity is presented which is useful for correlating drag data for circular and rectangular cylinders, normal flat plates with and without splitter plates, wedges, and v-gutters.

Keywords: Wake; Drag; Boundary; Cylinder; Wedge; Plate; Splitter plate

1. Introduction

The long distances traveled by golf balls have been generally explained in terms of high momentum transport from the turbulent, unseparated boundary layer (see Davies 1949). The drag reducing capability of riblets (see Walsh and Lindemann 1984, Coustols 1996) has likewise been explained in similar terms. However, Djenidi *et al.* (1994) found that appropriately sized riblets reduce frictional drag in laminar flows as well, at least on a per unit of wetted length basis. The most generally accepted explanation is that conditions along the upstream boundary layer, such as surface roughness, increase turbulence and thereby reduce drag (see, e.g., Granger 1995, p. 785). Bloor (1964), however, found that as Reynolds number increases, turbulence creeps into the wake towards the body from far downstream rather than from upstream. Moreover, the measurements of Cantwell and Coles (1983) show that the entire wake can be made fully turbulent and yet the upstream boundary layer remain laminar and forward on the body. Therefore, the condition of the upstream boundary layer may be *associated* with an increase in turbulence in the wake bubble, but it seems not to be the direct cause of the turbulence. What the upstream boundary layer is a direct cause of, however, is vorticity in the wake. This paper proposes a new quantity useful in correlating aerodynamic drag of bluff bodies to flow properties of the near wake. In the context of bluff-body flows, the quantity is the ratio of the kinetic energy (mean, periodic, and turbulent) to the vorticity in the wake of the body.

Early discussions on the enhanced flying characteristics of spinning projectiles, enabled, for example, by the rifling of a gun barrel, focused primarily on gyroscopic stability (Milne-Thomson 1968 p. 558; Thwaites 1960, p. 418). The improvements to the aerodynamic characteristics of the spinning Frisbee were attributed to spoilers that “disrupt the airflow”

* inquiries@mortonresearch.org

and “create a turbulent unseparated boundary layer over the convex side of the saucer and... result in a reduction of drag especially in high-speed flight and an increase in stability while in flight” (Headrick 1965). This description parallels the classical explanation of drag reduction wherein the drag coefficient of a body is reduced due to a tripping of the boundary layer to turbulent flow via high momentum mixing. This added momentum is said to cause the boundary layer to remain attached farther downstream on the body surface. It is clear that a lack of separation improves the drag characteristics of a body. The question remains as to what causes the lack of separation. The phrase “high momentum mixing” to explain this phenomenon has not generally proved to be extremely useful from a predictive standpoint. More recent ring designs, based on the Frisbee concept, with a bulk of material along the outer radius, appear to have even smaller drag coefficient. The enhanced flying characteristics of these designs are often attributed to the “spoiler” material on the outer rim. However, an equal, if not greater, affect of the massive outer rim is likely the prolonged rotation sustained by its flywheel affect. As noted by Potts and Crowther (2002), the distance record for a thrown Frisbee now stands at 250m. The distance record for any hand thrown object was set at 406.29m in 2003 using the Aerobie Pro Ring and then at 427.2m by Schummy (2005) using a boomerang. It seems unlikely that any non-rotating object could be thrown such distances, regardless of its shape or stability. Compare the above facts, for example, with the distance record for the javelin set at 98.48m in 1996.

One of the more subtle but curious contributions provided by CFD studies in the last few decades has been the placing on fairly firm footing the idea that, under certain conditions, rotation of a cylinder not only generates lift (Magnus 1852) but also reduces drag (see, e.g., Swanson 1961, Tanaka and Nagano 1972, Ingham 1983, Diaz *et al.* 1985, Badr *et al.* 1989, Ingham and Tang 1990, D’Alessio and Dennis 1994, Kang and Choi 1999, Stojković *et al.* 2002, Stojković *et al.* 2003, Inoue *et al.* 2003, Mittal and Kumar 2003). Spin-induced drag reduction in golf balls has been reported in the experimental studies of Aoki *et al.* (1998) and Aoyama (1998).

The major difficulty in theoretically predicting the flow properties for bluff-body flow problems lies in the separated boundary layer. Specific problems encountered when trying to apply conventional boundary layer theory to separated boundary layers include: a lack of knowledge of the proper far stream pressure boundary condition along the surface leading up to separation, uncertainty as to the location of the point of separation, and uncertainty as to the pressure at which separation occurs.

Models of the wake aimed at predicting drag are numerous (Kirchhoff 1869, Joukowski 1890, Riabouchinsky 1920, McNown and Yih 1953, Roshko 1954, Lavrentiev 1962, Wu 1962, Parkinson and Jandali 1970, Wu 1972, Yeung and Parkinson 1997). These rely heavily on a knowledge of the shape of the body in question. The closed wake model suggested by Batchelor (1956) focused primarily on finding the external flow past regions of uniform vorticity (see Childress 1966, Sadovskii 1971, Turfus 1993). Roshko (1993) derived an

expression for the length of the mean wake bubble in terms of the base suction coefficient and Reynolds shear stress for a normal flat plate with a trailing splitter plate. Using the free streamline model, Roshko was then able to predict a reasonable value for the drag coefficient. However, it is difficult to extend the model to a wake without a splitter plate that experiences vortex shedding (Roshko 1993; Williamson 1996). Balachandar *et al.* (1997) conducted a thorough review of past wake models and presented detailed contours of flow properties in the wake of cylinders (circular and rectangular) as well as flat plates.

Correlations of drag versus flow speed for a given bluff-body shape are complicated by factors such as flow transitions, surface roughness effects, and the choosing of the proper characteristic length and area to be used in the Reynolds number and drag coefficient. Rotation effects present an added difficulty. For these reasons, no single correlation, empirical or otherwise, has been found to relate drag force to flow speed for different body shapes and for all flow speeds.

2. An Integral Quantity Characterizing Vortices

In many bluff-body flow problems, general characteristics of the velocity field are fairly well known, at least in the region most critical to drag prediction, i.e., the wake bubble. In fact, the common trait among bluff-body flows appears to be the existence of a wake bubble in the time-mean flow field. For these reasons, a drag correlation will be proposed that involves an integral property of the mean wake vortex, that is, either of the symmetric time-mean vortices in the wake bubble.

Drag can be studied qualitatively by comparing the drag characteristics of two limiting extremes. Figure 1 shows a bluff body that experiences significant drag, and Figure 2 shows a knife edge that is assumed to experience no drag force. Naturally, the case in Figure 2 does not occur in reality, but any generally applicable drag correlation should exhibit the proper behavior in the limiting case represented by Figure 2. Therefore, the two conceptual extremes of Figures 1 and 2 will help to reveal the functional form of the drag correlation.

The application of the drag correlation to follow (see (1)) will require a clear distinction between the definition of the fluid domain and that of the fluid boundary. The strict mathematical definition of a boundary would stipulate a set of points forming an infinitely thin layer of fluid around the body. In contrast, Prandtl's boundary *layer* is of finite thickness and extends to the locus of points where the velocity has reached, say, 95% or 99% of its asymptotic (ideal flow) value. The boundary layer concept has proven to be extremely valuable; however, in the context of bluff-body flows, it may not be ideal. In the present work, the term *boundary* will refer to neither of the above definitions, but rather to all fluid possessing vorticity. In bluff body flows at appreciable Reynolds numbers, this will coincide closely with the fluid enveloped by closed streamlines.

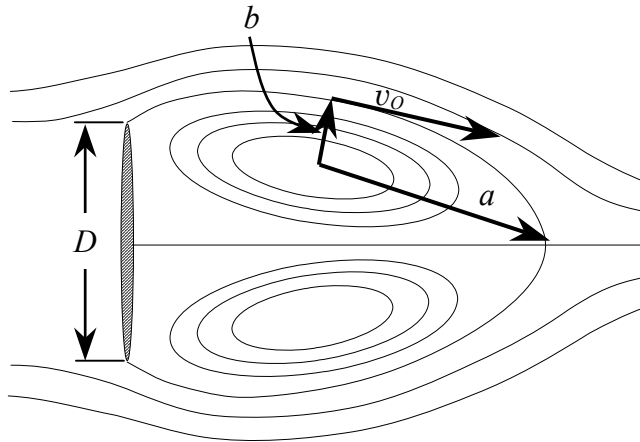


Figure 1. Schematic of flow past a normal flat plate.

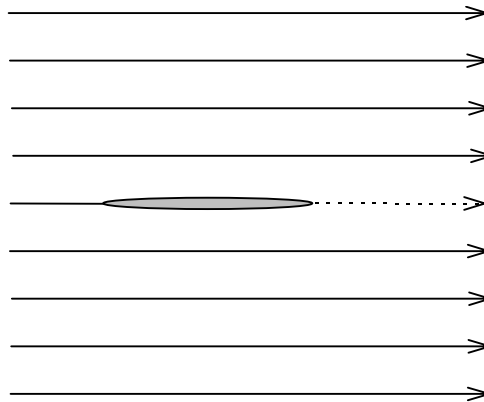


Figure 2. Schematic of flow past a knife edge.

Consider Figure 1 to represent a stationary body in a wind tunnel in which force is transmitted from the wind tunnel walls to the body. The wake bubble is the effect of this force that has been transmitted from the stationary body to the boundary of the fluid, but which *has not yet entered the fluid domain*. The energy is still contained within the boundary, which, for Figure 1, is of finite thickness, i.e., the extent of the mean wake bubble. In this case, the thickness of the boundary, as defined here, is finite; the vorticity within the boundary is finite; and a drag force exists.

If the wake size were to somehow decrease with v_0 held constant, the average vorticity in the boundary would obviously increase. Consider Figure 2 to be the limit of this wake reduction process. The result is irrotational flow external to the now infinitely thin boundary. The distinction with previous definitions of the term “boundary” is that even in ideal flow, a “boundary,” as defined here, still exists, albeit with only one streamline – the one that defines the body contour. Prandtl’s boundary layer, on the other hand, does not exist in such a flow.

If a fluid boundary is to exist in this limiting case, the abrupt change in velocity at the fluid/body interface requires that the vorticity within that boundary be infinite. Therefore, the case of zero drag, i.e., ideal flow, corresponds to infinite vorticity in the fluid boundary. Skin friction drag and form drag are contained within the two extremes of Figures 1 and 2.

From a qualitative understanding of the drag in Figures 1 and 2, an infinite vorticity in the boundary of a fluid domain is seen to correspond to inviscid flow. Consequently, for a given free stream velocity, aerodynamic drag is inversely proportional to the vorticity within the boundary of the fluid. Part of the reason for this counterintuitive result is due to the redefinition of the term *boundary*.

The following quantity is proposed for study:

$$G = \int_{\mathcal{V}} \frac{e_K}{\omega} d\mathcal{V}, \quad (1)$$

where e_K is the kinetic energy of the fluid per unit volume and ω is the vorticity magnitude within the volume, \mathcal{V} , of the boundary as defined above. If the boundary volume is not defined strictly as done earlier, then G can be undefined if applied in regions external to the wake bubble, where $\omega = 0$. Neither Prandtl's boundary layer nor the mathematical definition of a boundary resolve this problem suitably.

The quantity G is calculated for various shapes in Table 1. For the steadily rotating, non-translating rigid bodies shown in Table 1, as well as the elliptical patch of uniform vorticity, the following relation is found to hold:

$$G = \frac{1}{4}L, \quad (2)$$

where L is the angular momentum of the body or material. The relation in (2) appears not to be a kinematic identity because, as seen from Table 1, it is not true for the spherical vortex. The following relation, however, does hold for the spherical vortex as well as the solid cylinder and the elliptical patch of uniform vorticity in planar flow:

$$L = \dot{m}S, \quad (3)$$

where S is the cross-section area of the vortex containing a mean circulating flow rate of \dot{m} . The mass flow rate \dot{m} is that passing through the area $A = bW$, where W is the length of the vortex into the page (see Figure 1); therefore, $\mathcal{V} = 2SW$ for a pair of identical vortices. The relation in (3) naturally holds regardless of the type of material enclosed.

Observe from Table 1 that for the elliptical patch of uniform vorticity, the number G/S (as well as G/\mathcal{V}) is independent of the ellipticity of the vortex cross section. Note that for all but the spherical vortex, the ratio \dot{m}/m is the frequency of rotation. For the spherical vortex, the frequency is spatially dependent and goes to infinity on the bounding streamline due to the two stagnation points on that streamline.

| Config. | \dot{m} | $\frac{\dot{m}}{m}$ | $G = \int \frac{e_K}{\omega} dV$ | $L = \int \mathfrak{l} dV$ | $\frac{G}{L}$ |
|--------------------------------------|---------------------------------|-----------------------|--|--|----------------|
| Elliptical vortex patch | $\frac{1}{2} \rho v_o b W$ | $\frac{v_o}{2\pi a}$ | $\frac{1}{8} \rho v_o \pi a b^2 W$ | $\frac{1}{2} \rho v_o \pi a b^2 W$ | $\frac{1}{4}$ |
| Solid Cylinder (radius= b) | $\frac{1}{2} \rho v_o b W$ | $\frac{\Omega}{2\pi}$ | $\frac{1}{8} \rho v_o \pi b^3 W$ | $\frac{1}{2} \rho v_o \pi b^3 W$ | $\frac{1}{4}$ |
| Solid Cone (base = b height= h) | $\frac{1}{6} \rho \Omega b^2 h$ | $\frac{\Omega}{2\pi}$ | $\frac{1}{40} \rho \Omega \pi b^4 h$ | $\frac{1}{10} \rho \Omega \pi b^4 h$ | $\frac{1}{4}$ |
| Solid spinning Sphere | $\frac{2}{3} \rho \Omega R^3$ | $\frac{\Omega}{2\pi}$ | $\frac{2}{15} \rho \Omega \pi R^5$ | $\frac{8}{15} \rho \Omega \pi R^5$ | $\frac{1}{4}$ |
| Solid Torus ($R_C \geq r_o$) | $\rho A \Omega R_C$ | $\frac{\Omega}{2\pi}$ | $\frac{\rho \Omega A C}{4} \left[\frac{3}{4} r_o^2 + R_C^2 \right]$ | $\rho \Omega A C \left[\frac{3}{4} r_o^2 + R_C^2 \right]$ | $\frac{1}{4}$ |
| Hill's spherical vortex | $\frac{\pi}{4} \rho v_o R_o^2$ | $\frac{3v_o}{16R_o}$ | $\frac{\rho \pi^2 v_o R_o^4}{30}$ | $\frac{\rho \pi^2 v_o R_o^4}{8}$ | $\frac{4}{15}$ |

Table 1. Integral properties of rotating material in various shapes. (W is the length along the symmetry axis, $\Omega = v_o / b = v_o / R_o = v / R$, rotation is about the symmetry axis, $\mathfrak{l} = R \times \rho v$, ρ and m are the density and mass of the material, respectively. For the torus: $A = \pi r_o^2$ is the torus cross-section area, and $C = 2\pi R_C$ is the circumference of the core circle. For Hill's spherical vortex, R_o is the sphere radius.)

3. Drag Relation

As the wake bubble becomes fully turbulent with increasing Reynolds number, the drag correlation involving the quantity $\dot{m}S$ in (3) breaks down, while the one involving the quantity on the left side of (2) remains valid. A discussion of why this may be is given in §7.3. According to Table 1, (2) cannot be assumed valid generally. However, in the present study, only two-dimensional bodies are considered; therefore, the spherical vortex is not immediately relevant.

The integration in (1) is carried out over the time-mean wake vortex, i.e., the fluid boundary. Flows containing only one closed streamline, namely that coinciding with the contour of the body itself in ideal flow, produce no drag due to the infinite vorticity in the boundary. The experimental data in Figure 3 suggest the following relationship:

$$F_D = \frac{k v_\infty G}{2S}, \quad (4)$$

where the force, F_D , is the projection of the total force parallel to the free stream velocity v_∞ , and the factor of 1/2 will be absorbed later into the drag coefficient (see (7)).

This relation predicts a reduction in drag with increasing vorticity in the wake, as dictated by Figure 2. It also suggests that a reduction in drag may be possible by increasing the vorticity in the wake of the body, such as by spinning the body appropriately.

In the case of laminar wake bubbles, (2) can be substituted into (4) to see that the drag coefficient is proportional to \dot{m}/\dot{m}_∞ , where \dot{m} is the flow rate of mass recirculating in the wake bubble, and \dot{m}_∞ is the flow rate of mass that would otherwise pass, with velocity v_∞ , through the projected area made by the semi-minor axis of the wake vortex.

The drag correlation can also be formulated by using Newton's law, $F = m\dot{v}$, as a form for the correlation, assuming that the mass of fluid trapped in the wake vortex is constant. This allows a force to be associated with the mass, m , rotating in the wake vortex (assumed circular for the moment) having a radial acceleration given by $\dot{v} = \Omega v$. The drag correlation therefore becomes:

$$F_D \sim m\Omega v.$$

Here, m can be replaced (using Table 1) with $m = \dot{m}/f$, where the frequency f is given by $\Omega/(2\pi)$. Making this substitution gives:

$$F_D \sim 2\pi \dot{m} v. \quad (5)$$

From (3), this is equivalent to:

$$F_D \sim 2\pi \frac{L}{S} v,$$

and by (2), we have the form for the drag correlation:

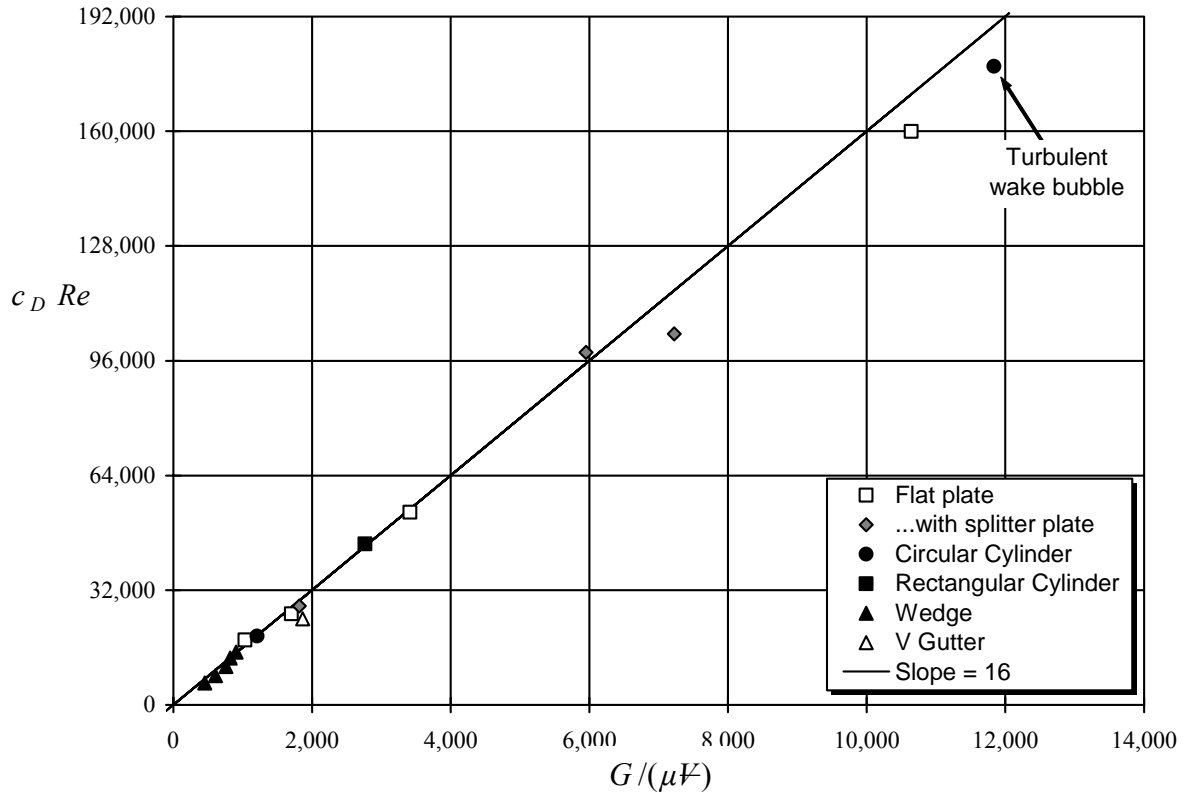
$$F_D \sim 8\pi \frac{G}{S} v. \quad (6)$$

Compare this relation with (4). Correlating bluff-body drag with the radial acceleration in the wake vortex, as done here to obtain (6), might have been anticipated from the fact that the force is acting against the back side of the body where the wake vortex is located.

Equation (4) may be cast in the form:

$$c_D Re = k \frac{G}{\mu \mathcal{V}} \quad (7)$$

where μ is the fluid viscosity, and \mathcal{V} is the vortex volume. The quantity $c_D Re$ will be referred to as the *dimensionless drag*. Figure 3 shows the correlation of dimensionless drag vs. $G/(\mu \mathcal{V})$ for available whole-field data in nominally two-dimensional flows. Here, the



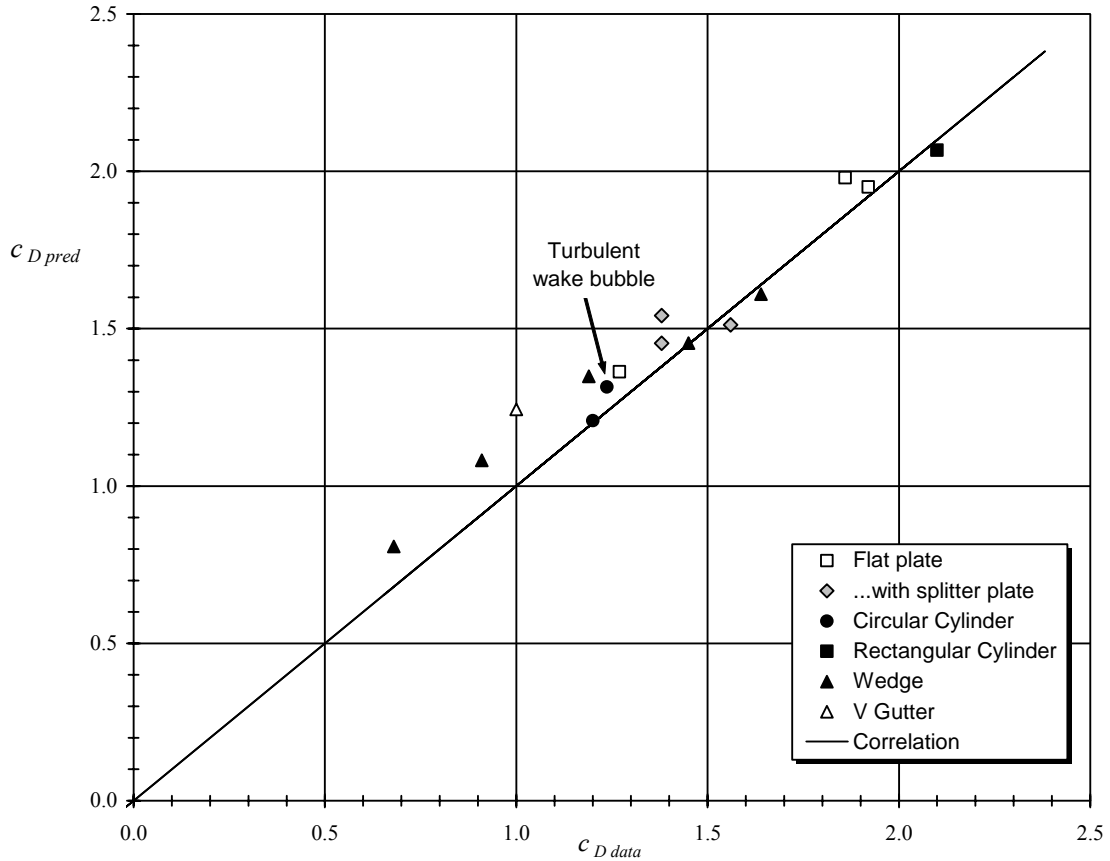


Figure 4. Correlation of predicted values of c_D , with available data listed in Table 2

4. Evaluating G in a Planar Wake Vortex

4.1. Velocity, Pressure, and Vorticity Fields

Equation (4), together with the calculation of G that follows, will allow the drag coefficient of a body to be determined from a velocity specified experimentally at the vortex perimeter and a dimension of the mean wake bubble. The mean velocity field can then be determined from the analytical solution for the flow in the wake bubble. For the nominally two-dimensional flows considered, the coherent or time-mean velocity component can be approximated by using the velocity field within a pair of elliptical patches of uniform vorticity (see Morton 1997). For flows exhibiting vortex shedding, the time average in the near wake remains a pair of counter-rotating vortices. The velocity field in an elliptical patch of uniform vorticity is, in rectangular coordinates,

$$\mathbf{v} = \begin{bmatrix} -y \\ \left(\frac{b}{a}\right)^2 x \end{bmatrix} \Omega_o. \quad (8)$$

| Study | Geometry | Re | β | AR | St | a/D | b/D | v_0/v_∞ | C_D Pred | C_D Data |
|------------------------------|--|---------|---------|------|--------------------|-------|-------------------|----------------|-------------------|-------------------|
| Arie & Rouse (1956) | Normal plate & splitter plate | 75,000 | 8.3% | 12 | | | 0.47 | 0.82 | 1.54 | 1.38 ^a |
| Castro & Haque (1987) | Normal plate & splitter plate | 23,000 | 6.5% | 12.4 | | | 0.46 | 0.79 | 1.45 | 1.38 ^b |
| Ruderich & Fernholz (1986) | Normal plate & splitter plate ^c | 32,000 | 10% | 22 | | | 0.6 ^d | 1.15 | 2.75 | n.a. |
| Good & Joubert (1968) | Normal fence in boundary layer | 63,000 | 9% | 11 | | | 0.72 | 1.05 | 1.51 ^e | n.a. |
| Perry & Steiner (1987) | Flat plate | 20,000 | 24.6% | 9.4 | 0.17 | 1.1 | 0.29 | | 1.36 | 1.27 ^f |
| Leder & Geropp (1993) | Flat plate | 28,000 | 8.5% | n.a. | 0.14 | 1.32 | 0.42 | | 1.95 | 1.92 |
| Fail <i>et al.</i> (1957) | Flat plate | 86,000 | 2.6% | 29 | 0.145 | 1.6 | 0.33 | 0.75 | 1.92 | 1.86 ^g |
| Bradbury (1976) | Flat plate ^h | 25,000 | 10% | 15 | | | 0.36 | 0.9 | 2.59 | n.a. |
| Bachalo <i>et al.</i> (1993) | Cylinder | 16,000 | 16.4% | 6.1 | 0.19 | 1.15 | 0.22 | | 1.21 | 1.20 |
| Cantwell & Coles (1983) | Cylinder | 144,000 | 4% | 29 | 0.179 | 0.43 | 0.12 | | 1.31 | 1.237 |
| Lyn <i>et al.</i> (1995) | Rectangular Cylinder | 21,400 | 7% | | 0.132 | | 0.34 ⁱ | 0.76 | 2.07 | 2.1 |
| Okamoto <i>et al.</i> (1977) | Wedge: | | | | | | | | | |
| | $\alpha = 15$ | 9,000 | 2.5% | 40 | 0.245 | 0.525 | 0.25 | | 0.81 | 0.68 |
| | $\alpha = 30$ | 9,000 | 2.5% | 40 | 0.24 | 0.69 | 0.26 | | 1.08 | 0.91 |
| | $\alpha = 60$ | 9,000 | 2.5% | 40 | 0.214 | 0.88 | 0.285 | | 1.35 | 1.19 |
| | $\alpha = 90$ | 9,000 | 2.5% | 40 | 0.179 | 1.01 | 0.32 | | 1.45 | 1.45 |
| | $\alpha = 120$ | 9,000 | 2.5% | 40 | 0.164 | 1.1 | 0.355 | | 1.61 | 1.64 |
| | $\alpha = 180$ | 9,000 | 2.5% | 40 | 0.143 | 1.25 | 0.41 | | 1.84 | 2.01 |
| Yang & Tsai (1992) | V Gutter (30°) | 24,000 | 20% | 5 | 0.225 ^j | 0.55 | 0.4 | | 1.24 | 1.0 ^k |

Table 2. Comparison between the drag coefficient of various two-dimensional bodies and the values predicted by (21). $Re > 9,000$.

^a This value obtained by Arie & Rouse omits the drag of their long (10 D) splitter plate by virtue of the location at which they measured the downstream pressures in their drag integral.

^b This value by Arie & Rouse (1956) omits the drag of the splitter plate (17 D in this case).

^c Length of splitter plate = 30 D . Ruderich & Fernholz intentionally tested with very high free stream turbulence (~30%).

^d According to Figure 8 of Castro & Haque (1987), velocity profiles appear to cross at the common value of v_0 at the vertical distance b from vortex centre to the wake bubble boundary. This fact was used to determine b from Figures 15 of Ruderich & Fernholz (1986). Figure 16 was then use to find v_0 .

^e The correlation value was divided in half because only one vortex was present.

^f Taken from Fail *et al.* (1957) data for appropriate aspect ratio.

^g Their value of 1.96 based on Fage & Johansen (1927) was corrected for blockage by Fail *et al.* (1957) using Maskell's method (see Maskell 1965).

^h Bradbury intentionally tested with very high free stream turbulence. Vortex shedding is assumed here ($\delta = 1$), though no Strouhal number or drag coefficient was reported in the study.

ⁱ Can be found by locating in Figure 3 of Lyn *et al.* (1995) where \bar{v}^t reaches a minimum and subtracting from the location where the streamwise velocity, \bar{u}^t , is zero, also in Figure 3 of the paper.

^j Yang *et al.* (1994).

^k Hoerner (1965) p. 3-18.

Here, a and b are, respectively, the semi-major and semi-minor axes of the vortex, and Ω_O is the rotation rate (about the vortex center) of a fluid particle at the point where the semi-minor axis intersects the perimeter of the vortex. Therefore, the velocity at that point on the perimeter is $v_O = \Omega_O b$. Alternatively, in streamline coordinates, given by (Morton 1997):

$$x = \bar{x}^1 A \cos(\bar{x}^2) \quad y = \bar{x}^1 B \sin(\bar{x}^2) \quad z = \bar{x}^3 \quad (9)$$

the non-zero component of the velocity tensor is:

$$\bar{v}^2 = \frac{v_O}{a}. \quad (10)$$

The pressure field in the vortex is (see Morton 1997):

$$p - p_C = \frac{1}{2} \rho (\Omega_O r)^2 \left(\frac{b}{a} \right)^2, \quad (11)$$

where p is the pressure at a distance r from the vortex center where the pressure is p_C . Therefore, pressure contours are circular, regardless of the ellipticity of the vortex cross section. The constant vorticity of an elliptical patch of uniform vorticity in planar flow is (see Morton 1997)

$$\omega = \bar{v}^2 \left(\frac{a}{b} + \frac{b}{a} \right), \quad (12)$$

or

$$\omega = \frac{v_O}{b} \left[1 + \left(\frac{b}{a} \right)^2 \right]. \quad (13)$$

4.2. Evaluating G

The ratio G to be used in (4) can be found by adding the turbulent kinetic energy per unit volume, e_{TK} , and the mean kinetic energy, e_{MK} , as follows:

$$G \equiv \int_{\mathcal{V}} \frac{e_K}{\omega} d\mathcal{V} = \int_{\mathcal{V}} \left(\frac{e_{MK} + e_{TK}}{\omega} \right) d\mathcal{V}. \quad (14)$$

The standing eddies in bluff-body wakes naturally occur in pairs, and if these are considered to be a single vortex ring infinitely long into and out of the page, the kinetic energy is doubled. For a pair of identical vortices, therefore,

$$G = 2 \int_{\mathcal{V}} \left(\frac{e_{MK} + e_{TK}}{\omega} \right) d\mathcal{V}. \quad (15)$$

One need not consider ω to be the *absolute value* of vorticity in order to account of the

vorticity of opposite signs in the wake, provided one considers the volume of each half of the wake to be oriented in the opposite direction to that of its adjacent volume. Expanding (15) gives

$$G = \int_0^W \int_0^{2\pi} \int_0^{\bar{x}_{\max}^1} \frac{\bar{g}_{22} (\bar{v}^2)^2}{\sqrt{\bar{g}_{33}} \bar{\omega}^3} \sqrt{\bar{g}} d\bar{x}^1 d\bar{x}^2 d\bar{x}^3 + \int_{eddy} \frac{\left(\langle u_1'^2 \rangle + \langle u_2'^2 \rangle + \langle u_3'^2 \rangle \right)}{\omega} d\mathcal{V},$$

where, for the streamlined coordinate system, $\bar{g}_{33} = 1$, $\sqrt{\bar{g}} = \bar{x}^1 AB$, $\bar{\omega}^3$ is the constant given by (12) or (13), and $\bar{g}_{22} = (\bar{x}^1)^2 (A^2 \sin^2(\bar{x}^2) + B^2 \cos^2(\bar{x}^2))$. The velocity components marked with primes indicate the random fluctuations of the respective components, and the overbar indicates averaging. According to (10), \bar{v}^2 is constant and can be brought out of the integral on the right. The result for the pair of vortices is:

$$G = \frac{1}{4} \rho v_O b \mathcal{V} + \frac{\rho v_\infty^2}{\omega} k_T \mathcal{V}, \quad (16)$$

where \mathcal{V} is the vortex volume and

$$k_T \equiv \frac{1}{\mathcal{V}} \sum_i \left(\frac{\langle u_1'^2 \rangle}{v_\infty^2} + \frac{\langle u_2'^2 \rangle}{v_\infty^2} + \frac{\langle u_3'^2 \rangle}{v_\infty^2} \right) \Delta \mathcal{V}_i. \quad (17)$$

Notice from (16) that when turbulent kinetic energy is negligible in the wake vortex, G/S is independent of the axis ratio of the cross section of the elliptical vortex and that it is equal to half the mass flow rate through any semi-axes of the pair of vortices. That is:

$$\frac{G_M}{S} = \frac{\dot{m}}{2}. \quad (\text{planar, laminar}) \quad (18)$$

Therefore the ratio is invariant with respect to the axis ratio of the vortex cross section, provided the semi-minor axis and perimeter velocity, v_O , remain unchanged.

5. Drag Relation

The drag coefficient can be determined by substituting (16) into (7), giving:

$$c_D = 8 \frac{b}{D} \left[\frac{v_O}{2v_\infty} + \frac{2v_\infty}{v_O} \frac{k_T}{(1+(b/a)^2)} \right]. \quad (19)$$

Here, the characteristic length, D , is the projected body dimension normal to the free stream and is used in the Reynolds number. In all values of Table 3 except for those of Cantwell and Coles (1983) (which will be discussed in §6 and §7), the turbulent transition waves had not penetrated into the wake vortex so that $k_T = 0$ in those cases. If the velocity ratio appearing in (19) is not known, it can often be related to the shedding frequency by a Strouhal number

grouping derived from the elliptical vortex patch (see Appendix). The necessary relation is repeated below:

$$\frac{v_O}{v_\infty} = \frac{2\pi a}{nD} St. \quad (20)$$

Here, St is the classical definition of the Strouhal number, and n is the number of vortices shed downstream per shedding cycle, namely 2. Equation (20) can be employed to write (19) in terms of the Strouhal number rather than the vortex perimeter velocity ratio. With the onset of vortex shedding, however, the energy becomes split into a mean component and a periodic component. The mean wake bubble dramatically decreases in size with the removal of a splitter plate. This is clearly demonstrated by Hwang *et al.* (2003) at lower Reynolds number. If the correlation for the drag coefficient, (19), is modified to so as to fit the data with and without splitter plates, the following form is obtained:

$$c_D = 8 \frac{b}{D} \left[(1 + \delta) \frac{v_O}{2v_\infty} + \frac{2v_\infty}{v_O} \left(\frac{k_T}{1 + (b/a)^2} \right) \right]. \quad (21)$$

When vortex shedding is absent due to the presence of a splitter plate and the attendant large wake bubble, $\delta = 0$; and when vortex shedding is present and the mean wake bubble shrinks, $\delta = 1$. Therefore, kinetic energy of the mean flow appears to be doubled when the splitter plate is removed, the additional portion being in the form of vortex shedding. Since the mean kinetic energy is calculated based on the now smaller time-mean wake bubble, the kinetic energy due to vortex shedding must be included by using δ .

Using (21), drag predictions can be made from steady or time-mean wake flow visualizations; however, the perimeter velocity, v_O , must be measured experimentally. The dimensionless distance, b/D , to this point from the vortex center may then be found graphically from visualization of the mean flow (see Figure 1). Alternatively, using (20) the measured Strouhal number and dimensionless semi-major axis, a/D , of the wake vortex may be used in lieu of the velocity ratio.

6. Illustrative Example

The case to be examined is the set of cylinder experiments made by Cantwell and Coles (1983). The purpose of their experiment was to provide measurements of wake flow in which the separation point was laminar, yet the near wake region was fully turbulent. As it turns out, this strategy has provided an invaluable set of data, which allows (1) or (7) to be seen in a more general light.

In accordance with their objective stated above, Cantwell and Coles chose from a series of cases, one in which the Reynolds number was 1.44×10^5 so that the flow was on the brink

of entering the so called drag crisis. Bearman (1969) indicated the following values of the Strouhal number and drag coefficient on either side of this drag crisis:

| Re | c_D | St |
|-------------------|-------|------|
| 2×10^5 | 1.14 | 0.19 |
| 4.1×10^5 | 0.235 | 0.46 |

The mean velocity measurements of Cantwell and Coles (1983) prior to this drag crisis are shown in Figure 5 with a indicated. Since the velocity at the semi-minor axis of the wake vortex was not given, (20) will be used to estimate it. The drag coefficient is determined graphically by measuring the semi-axes of either of the wake vortices.

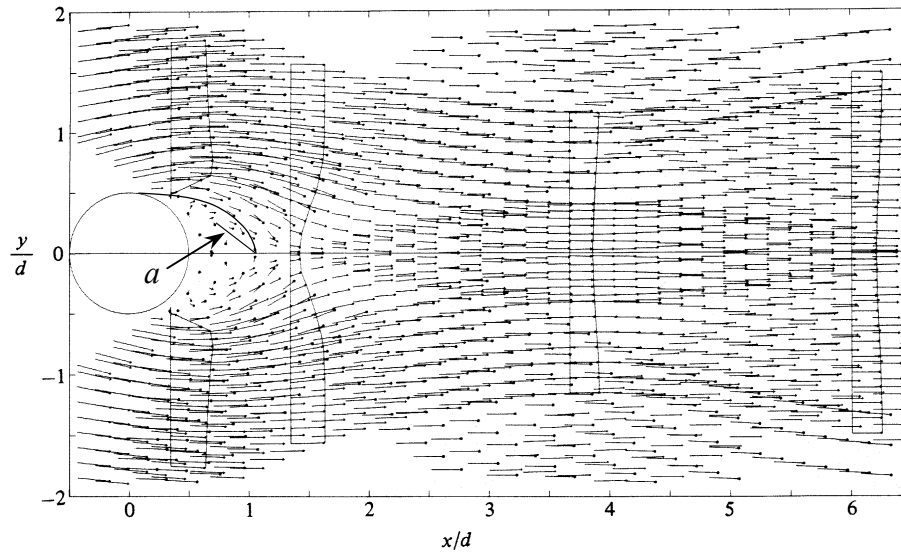


Figure 5. Mean velocity vectors in the wake of a circular cylinder. $Re = 144,000$, $AR = 25$, $\beta = 4\%$, $c_D = 1.237$, $St = 0.179$, $TL = 0.6\%$. (Cantwell and Coles 1983)

At this Reynolds number, the turbulent transition waves have penetrated the wake bubble. The result is a noticeable reduction in the size of the wake bubble and a dramatic increase in the *fluctuating* component of velocity. Measurements of the needed velocity fluctuations were also made by Cantwell and Coles. The turbulent kinetic energy in the wake bubble can be found using contours of $\langle v_1'^2 \rangle / v_\infty^2$ and $\langle v_2'^2 \rangle / v_\infty^2$, the global mean of the random fluctuations shown (with overbars) in Figures 27(b) and 28(b) of their paper. The remaining quantity, $\langle v_3'^2 \rangle / v_\infty^2$, will be assumed to be an average of these two. The Reynolds normal stress contours appear similar to those presented by Balachandar *et al.* (1997) for a cylinder wake bubble at low Reynolds number. From these and Figure 5 above, the semi-axes of the vortices are found graphically to be $a/D \approx 0.43$ and $b/D \approx 0.12$. Applying (17) graphically to Figures 27(b) and 28(b) of Cantwell and Coles (1983) shows that $k_T = 0.147$.

The velocity ratio v_O/v_∞ can be found using (20):

$$\frac{v_O}{v_\infty} = \frac{2\pi(0.43)}{2} 0.179 = 0.242.$$

The drag coefficient can then be estimated by (21), as follows:

$$c_D = 8 \frac{b}{D} \left[(1 + \delta) \frac{v_O}{2v_\infty} + \frac{2v_\infty}{v_O} \frac{k_T}{(1 + (b/a)^2)} \right]$$

$$c_D = 8(0.12) \left[(1 + 1) \frac{0.242}{2} + \frac{2}{0.242} \frac{(0.147)}{(1 + (0.279)^2)} \right]$$

$$c_D \approx 1.31$$

The value measured by Cantwell and Coles was $c_D = 1.237$.

7. Discussion

7.1. The Drag Crisis

In the example shown, the drag coefficient remains large even after the increase in the turbulent kinetic energy within the wake bubble and the decrease in mean wake width. The drag coefficient finally decreases suddenly when the Reynolds number is increased still further into the range $2 \times 10^5 < Re < 5 \times 10^5$, known as the “drag crisis,” due to the well known shift in the location of the separation point. This shift causes the vorticity (the denominator of (1)) to increase suddenly. Recall that the Reynolds number in the Cantwell and Coles experiment was large enough for the mean wake bubble to become almost entirely turbulent, yet small enough to ensure that the separation point remain forward on the body. The range of Reynolds numbers for which this set of circumstances exists is narrow. At these unique conditions, the size of the wake bubble is much smaller than it is at slightly lower Reynolds numbers, for which the wake bubble is not fully turbulent. Therefore, as the Reynolds number is increased into this unique range, the increase in fluctuating kinetic energy in the wake bubble and the reduction in the size of the mean wake bubble occur simultaneously. The vorticity in the wake bubble, on the other hand, has not changed appreciably within this narrow range of Reynolds numbers because vorticity within the wake volume is a direct function of the distance traveled by the fluid through the boundary layer. The sudden reduction in the drag coefficient does not occur until the boundary layer extends to the rear of the cylinder, at an even higher Reynolds number. The distance traveled by the fluid in the boundary layer is then longer, the vorticity in the denominator of the drag relation (1) is therefore higher, and hence the drag coefficient suddenly decreases (see (7)). Therefore, the decrease in drag coefficient occurs at a slightly higher Reynolds number than does the decrease in wake size.

Situations do exist where advancement of the transition point forward on the body has the effect of reducing drag (see e.g., Coustols 1996, Gad-el-Hak & Bushnell 1991, Coustols and Schmitt 1990). However, this is accomplished by placing distributed roughness elements or riblets on the surface, which can themselves be viewed from the standpoint of increasing the vorticity in the fluid boundary and hence reducing the function G .

7.2. Extending the Correlation to Lower Reynolds Numbers

At lower Reynolds numbers, sufficient whole-field data does not exist to formulate a meaningful correlation owing to the complexity of the transitions in this regime. However, some of the most complete (for the purposes of the present study) works to date in the range $100 \leq Re \leq 300$, are listed in Table 3. For a description of the changes occurring in the wake near these Reynolds numbers, see Williamson (1996a) or (1996b) for the circular cylinder and Julien *et al.* (2003) for the flat plate. In order to better understand the three-dimensional behavior of flow in the near wake of a normal flat plate, Wu *et al.* (2005) analyzed the phase difference of vortex shedding at two different spanwise locations and found two distinct modes and very pronounced three-dimensionality. Note from Table 3 that just beyond the 3-D wake transition regime, the correlation appears to underpredict the drag coefficient by a factor of 2. Therefore, visual observation of the wake is clearly inadequate in regimes where there are changes in the nature of out-of-plane shedding. Instead of modeling the wake as an elliptical patch of uniform vorticity, the correlation in (4) could be better examined at these lower Reynolds numbers if (1) were evaluated directly as a post-processing procedure of DNS studies.

| Study | Geometry | Re | St | a/D | b/D | u_0/u_∞ | C_D Pred | C_D Data |
|----------------------------------|--|------|-------|-------|-------|----------------|------------|-------------------|
| Najjar & Balachandar (1998) | Flat plate (3D DNS) | 250 | 0.167 | 1.0 | 0.28 | | 1.17 | 2.36 |
| Dennis & Chang (1970) | Cylinder (2D Steady) | 100 | - | 4.5 | 0.33 | n.a. | | 1.34 |
| Hwang, <i>et al.</i> (2003) | Cylinder (2D Unsteady) | 100 | 0.164 | 0.92 | 0.23 | | 0.87 | 1.33 |
| Hwang, <i>et al.</i> (2003) | Cylinder & Slip Plate (2D Unsteady) | 100 | 0.137 | 1.8 | 0.28 | n.a. | 0.87 | 1.18 |
| Mittal (2003) | Cylinder & Slip Plate (2D Steady ^a) | 100 | - | | 0.32 | n.a. | | 1.065 |
| Protas & Wesfreid (2002) | Cylinder & Slip Plate (2D Steady ^a) | 150 | - | | 0.33 | 0.54 | 0.71 | 0.86 |
| Balachandar <i>et al.</i> (1997) | Cylinder (3D DNS) | 300 | 0.207 | 0.5 | 0.24 | | 0.61 | 1.27 ^b |

Table 3. Comparison between the drag coefficient of various two-dimensional bodies and the values predicted by (21). $100 \leq Re \leq 300$, $\beta = 0\%$, $AR = \infty$.

^a Unperturbed solution.

^b Wieselsberger (1922) obtained 1.22.

7.3. Turbulent Angular Momentum

For turbulent flows, the drag correlation is easier to evaluate using the left side of (2) than the right. It may be instructive, however, to substitute the right side of (2) into (4) to obtain:

$$F_D = 2v_\infty \frac{L}{S} \quad (22)$$

for each half of the wake bubble. Therefore, for a given velocity, a higher force causes a higher angular momentum per unit area. Turbulence may be an ideal mechanism for filling a region with concentrations of angular momentum to accommodate a large force. From Table 1 and (3), we can write

$$\dot{m} = \frac{L}{S} = \frac{1}{2} \rho v_o b W \quad (23)$$

for a cylindrical vortex, the cross section of which is depicted in Figure 6a. If the cylindrical vortex were replaced with two counter-rotating vortices as shown in Figure 6b while maintaining the same velocity magnitude at points of tangency, the length b would become half of what it was, as shown. There would be no gain in the storage capacity of angular momentum per unit area or mass flow rate because, while there are now twice as many vortices, the quantity L/S , which according to (23) scales with b , is cut in half for each vortex. If, however, the original vortex were replaced with four vortices as shown in Figure 6c, there would be a gain in storage capacity of angular momentum per unit area because b reduces to $b/(1+\sqrt{2})$, yet there are now $N=4$ vortices. Therefore, for this case the storage capacity has increased by a factor of $4/(1+\sqrt{2})$.

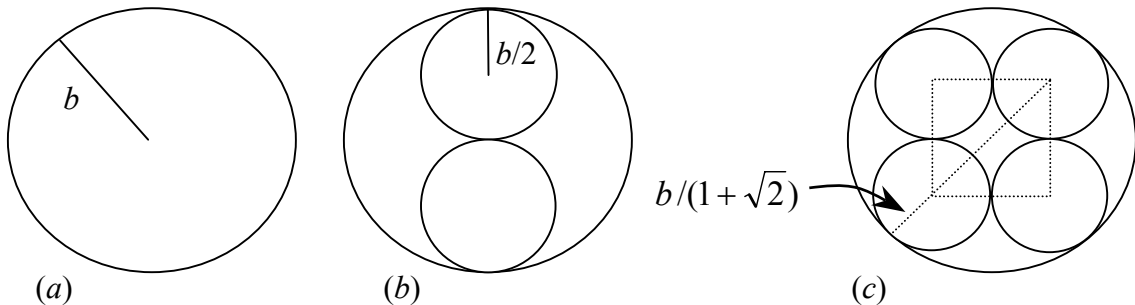


Figure 6. Model of the subdivision process of a single vortex into multiple smaller vortices. (a) $N=1$, (b) $N=2$, (c) $N=4$.

In the limit as the number of smaller vortices filling the area increases, that is, as $N \rightarrow \infty$, we find by equating the areas before and after this subdivision process that the radius, and hence the mass flow rate of each small vortex, scales as $1/\sqrt{N}$ so that the total storage capacity of angular momentum per unit area scales as \sqrt{N} . This indicates that the mass flow rate enclosed by the volume can increase without bound as the vortices become smaller.

If the initial region were to subdivide instead into spherical vortices, the mass flow rate would scale as R^2 according to Table 1. Equating the volumes before and after the subdivision process shows that the radius of each smaller spherical vortex scales as $1/N^{1/3}$. Therefore, the mass flow rate or angular momentum per unit area of each of these scales as $1/N^{2/3}$; and the total storage capacity of mass flow rate in the volume scales as $N^{1/3}$. Therefore, again, the mass flow rate increases without bound as the number of vortices in the sphere increases.

In general, therefore,

$$R \sim \frac{1}{N^{1/n}}, \quad (24)$$

$$\dot{m} = \sum_{i=1}^N \dot{m}_i = N\dot{m}_i \sim N^{1/n}, \quad (25)$$

where n is the dimensionality of the vortex, and R is the radius of the vortex, whether tubular ($n = 2$) or spherical ($n = 3$). Therefore, even though N is obviously greater for a packing of spherical vortices than for a packing of cylindrical vortex tubes of equal radius, as shown in the preceding two paragraphs, the mass flow rate in each of the N vortex *tubes* is greater than it is in each of the N *spherical* vortices, the general relation being: $\dot{m}_i \sim 1/N^{(n-1)/n}$. By substituting (24) into (25) it is clear that the two effects exactly compensate one another so that the total mass flow rate in the wake increases as $1/R$, where R is the radius of the small vortices, whether tubular or spherical.

In §3, it was stated that the drag correlation using \dot{m} broke down when applied to highly turbulent wake bubbles, while the correlation using G remained valid. This is because calculating \dot{m} for a turbulent wake bubble based upon Figure 6a is inaccurate, and counting turbulent eddies in the equivalent of Figure 6c is impractical.

In summary, substitution of (3) into (22) gives, for both halves of the wake bubble:

$$F_D = 4\dot{m}v_\infty, \quad (26)$$

where \dot{m} is the total mass flow rate circulating in eddies in the fluid boundary. With regard to the factor of 4 in this equation, it is possible that there is some energy mode, out of plane or otherwise, that has been systematically missed in the evaluation of each of the data points for the correlation. If so, a factor other than 4 would be required. If a relation such as (26) or (4) does turn out to be valid generally, not only would it relate drag to flow speed without the use of viscosity, but in the form of (26) it may be useful in turbulence modeling or as an eddy size criterion in large eddy simulation studies.

7.4. Analogies with Electromagnetism

The analogies between electromagnetic theory and fluid mechanics are numerous and well known (see, e.g., Milne-Thomson 1968 p. 574). Hsu (1976), for example, found the interesting fact that a tornado cannot be formed if the ground plane is removed. Therefore, the touchdown of a tornado resembles the arcing of an electric spark such as lightning. In light of (2) and (4), a few additional observations can be made. First, there are some interesting parallels between the quantity G of vortices and Planck's constant, h . Both are ratios of energy to frequency (since vorticity in (13) can be related to frequency using $\Omega_o = 2\pi f$), and both seem to describe angular momentum (Bohr 1913). It is well known that if Planck's constant were zero, there would be no quantum mechanics, a value of zero for h corresponding to classical mechanics. A value of zero for G corresponds to inviscid flow, for which the commutator of the velocity gradient, namely the vorticity, is zero everywhere except on infinitely thin boundaries. Fluid resistance becomes appreciable as separation vortices appear, and in metals, superconductivity is lost as soon as vortices appear (Abrikosov 1988, p. 456). Also, by multiplying (26) by velocity in order to obtain the power lost due to drag, one obtains a relation that resembles the I^2R losses in electrical power lines, the role of resistance being played by m in the fluid eddies. Finally, there are similarities between the free-stream velocity vector in bluff-body flow and the Poynting vector of an electromagnetic wave. Figure 7 illustrates the relation between the force, the net vorticity vector, and the fluid velocity of a two-dimensional bluff body. Incidentally, this figure also illustrates why the period of experimentally measured drag oscillation is typically half that of the lift oscillations. Drag occurs with the shedding of either of the two vortices, whereas lift only occurs with the shedding of one of them.

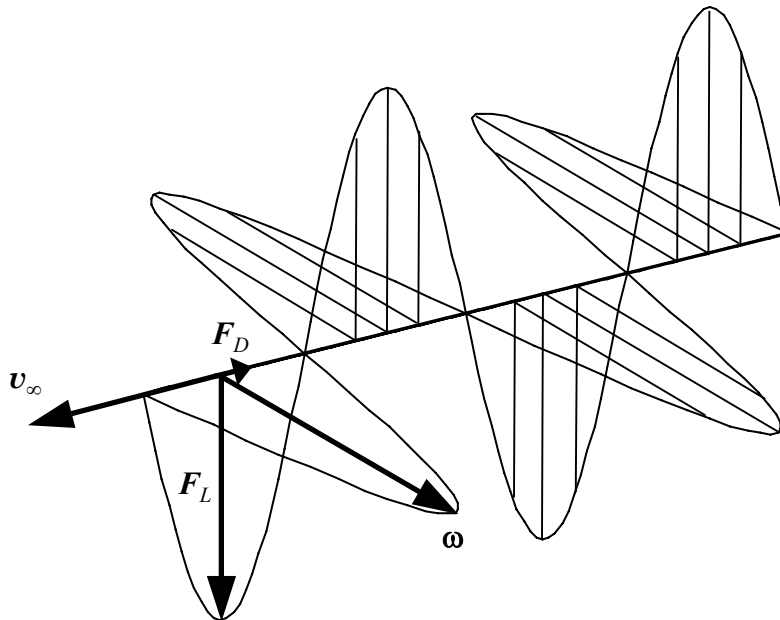


Figure 7. Plane polarized mean quantities F , ω , and v_∞ during vortex shedding past a prismatic bluff-body.

8. Conclusion

The drag of two-dimensional bodies appears to be correlated with the ratio of the kinetic energy to the vorticity in its wake, at least in the range $9 \times 10^3 \leq Re \leq 1.44 \times 10^5$. The fluid boundary, defined herein as any fluid possessing vorticity, specifies the volume over which the above ratio is to be evaluated. As a limiting case of the drag correlation, ideal flows possess infinitely thin boundaries and therefore infinite vorticity in these boundaries, and hence no drag. To aid in computing the required ratio from existing test data, a Strouhal number formulated using the elliptical vortex patch, can be used in lieu of the time-averaged velocity at a point on the vortex perimeter. The correlation indicates that the drag force on a body is proportional to the flow speed and the mass flow rate in the boundary of the fluid, i.e., the wake bubble. This mass flow rate can become unbounded as the scale of the contained vortices becomes finer.

REFERENCES

- Abrikosov, A. A., 1988 *Fundamentals of the Theory of Metals*, Elsevier Science.
- Aoki, K., Nakayama, Y., Hayasida, T., Yamaguti, N., & Sugiura, M., 1998 Flow Characteristics of a Golf Ball Using Visualization Techniques, in *Science & Golf III: Proceedings of the World Scientific Congress of Golf*, pp. 446-456, edited by Farrally & Cochran, Human Kinetics Publishers, London.
- Aoyama, S., 1998 The "Row Effect" Anomaly in the 336 Octahedron Dimple Pattern, in *Science & Golf III: Proceedings of the World Scientific Congress of Golf*, pp. 457-463, edited by Farrally & Cochran, Human Kinetics Publishers, London.
- Arie, M., & Rouse, H., 1956 Experiments on two-dimensional flow over a normal wall. *Journal of Fluid Mechanics* **1**, pp. 129-141.
- Bachalo, W. D., Bachalo, E. J., Hanscom, J. M., & Sankar, S. V., 1993 An Investigation of Spray Interaction With Large-Scale Eddies. *AIAA Paper No. 93-0696*, 19 pp.
- Badr, H. M., Dennis, S. C. R., & Young, P. J. S., 1989 Steady and unsteady flow past a rotating circular cylinder at low Reynolds numbers. *Computers & Fluids* **17**, pp. 579-609.
- Balachandar, S., Mittal, R., & Najjar, F. M., 1997 Properties of the mean recirculation region in the wakes of two-dimensional bluff bodies. *Journal of Fluid Mechanics* **351**, pp. 167-199.
- Batchelor, G. K., 1956 A proposal concerning laminar wakes behind bluff bodies at large Reynolds numbers. *Journal of Fluid Mechanics* **1**, pp. 388-398.
- Bearman, P. W., 1969 On vortex shedding from a circular cylinder in the critical Reynolds number régime. *Journal of Fluid Mechanics* **37**, pp. 577-585.
- Bloor, M. S., 1964 The transition to turbulence in the wake of a circular cylinder. *Journal of Fluid Mechanics* **19**, pp. 290-304.

- Bohr, N., 1913 On the Constitution of Atoms and Molecules. *Philosophical Magazine* **26**, pp. 1-25.
- Bradbury, L. J. S., 1976 Measurements with a pulsed-wire and a hot-wire anemometer in the highly turbulent wake of a normal flat plate. *Journal of Fluid Mechanics* **77**, pp. 473-497.
- Cantwell, B. J., & Coles, D., 1983 An experimental study of entrainment and transport in the turbulent near wake of a circular cylinder. *Journal of Fluid Mechanics* **135**, pp. 321-374.
- Castro, I. P. & Haque, A., 1987 The structure of a turbulent shear layer bounding a separation region. *Journal of Fluid Mechanics* **179**, pp. 439-468.
- Childress, S., 1966 Solutions of Euler's Equations containing Finite Eddies. *The Physics of Fluids* **9**, pp. 860-872.
- Coustols, E., 1996 Riblets: main known and unknown features. *Emerging techniques in drag reduction*, Mechanical Engineering Publications, London, edited by Choi, Prasad, and Truong, pp. 3-43.
- Coustols, E. & Schmitt, V., 1990 Synthesis of Experimental Riblet Studies in Transonic Conditions, in *Turbulence Control by Passive Means, Proceedings of the 4th European Drag Reduction Meeting*, Kluwer Academic Publishers, Dordrecht, edited by E. Coustols.
- D'Alessio, S. J. D. & Dennis, S. C. R., 1994 A vorticity model for viscous flow past a cylinder. *Computers & Fluids* **23**, pp. 279-293.
- Davies, J. M., 1949 The Aerodynamics of Golf Balls. *Journal of Applied Physics* **20**, p. 821-828.
- Dennis, S. C. R. & Chang, G.-Z., 1970 Numerical solutions for steady flow past a circular cylinder at Reynolds numbers up to 100. *Journal of Fluid Mechanics* **42**, pp. 471-489.
- Diaz, F., Gavaldà, J., Kawall, J. G., Keffer, J. F., & Giralt, F., 1985 Asymmetrical Wake Generated by a Spinning Cylinder. *AIAA Journal* **23**, pp. 49-54.
- Djenidi, L., Anselmet, F., Liandrat, J., & Fulachier, L., 1994 Laminar boundary layer over riblets. *Physics of Fluids* **6**, pp. 2993-2999.
- Fage, A. & Johansen, F. C., 1927 On the Flow of Air behind an Inclined Flat Plate of Infinite Span. *Proceedings of the Royal Society of London A* **116**, pp. 170-197.
- Fail, R., Lawford, J. A., & Eyre, R. C. W., 1957 Low-Speed Experiments on the Wake Characteristics of Flat Plates normal to an Air Stream. *Aeronautical Research Council, Reports and Memoranda* No. 3120.
- Gad-el-Hak, M. & Bushnell, D. M., 1991 Separation Control: Review. *ASME Journal of Fluids Engineering* **113**, pp. 5-30.
- Good, M. C. & Joubert, P. N., 1968 The form drag of two-dimensional bluff-plates immersed in turbulent boundary layers. *Journal of Fluid Mechanics* **31**, pp. 547-582.
- Granger, R. A., 1995 *Fluid Mechanics*, 2nd ed., Dover.
- Headrick, E. E., 1967 Flying Saucer. *U.S. Patent No. 3,359,678*.
- Hoerner, S. F., 1965 *Fluid-Dynamic Drag*, published by Hoerner Fluid Dynamics.

- Hsu, C. T. & Fattahi, B., 1976 Mechanism of tornado funnel formation. *The Physics of Fluids* **19**, pp. 1853-1857.
- Hwang, J.-Y., Yang, K.-S., & Sun, S.-H. 2003 Reduction of flow-induced forces on a circular cylinder using a detached splitter plate. *Physics of Fluids* **15**, pp. 2433-2436.
- Ingham, D. B., 1983 Steady flow past a rotating cylinder. *Computers & Fluids* **11**, pp. 351-366.
- Ingham, T. B. & Tang, T., 1990 A Numerical Investigation into the Steady Flow Past a Rotating Circular Cylinder at Low and Intermediate Reynolds Numbers. *Journal of Computational Physics* **87**, pp. 91-107.
- Inoue, O., Mori, M., & Hatakeyama, N., 2003 Control of aeolian tones radiated from a circular cylinder in a uniform flow. *Physics of Fluids* **15**, pp. 1424-1441.
- Joukowski, N. E., 1890 I - A Modification of Kirchhoff's Method of Determining a Two Dimensional Motion of a Fluid Given a Constant Velocity Along an Unknown Stream Line. II - Determination of the Motion of a Fluid for Any Condition Given on a Stream Line. *Rec. Math.* **25**, (also Collected Works of N. E. Joukowski, Vol. II, III, Issue 3, Trans. CAHI, No. 41, 1930.)
- Julien, S., Lasheras, J., & Chomaz, J.-M., 2003 Three-dimensional instability and vorticity patterns in the wake of a flat plate. *Journal of Fluid Mechanics* **479**, pp. 155-189.
- Kang, S. & Choi, H., 1999 Laminar flow past a rotating circular cylinder. *Physics of Fluids* **11**, pp. 3312-3321; 2000 Erratum. *Physics of Fluids* **11**, pp. 239.
- Kirchhoff, G., 1869 Zur Theorie Freier Flüssigkeitsstrahlen. *Journal fuer die reine und angewandte Mathematik (Crelle)* **70**, pp. 289-298.
- Lavrentiev, M. A., 1962 The Variational Method in Boundary Problems for Systems of Equations of Elliptic Type. *Akademi Nauk SSSR Moscow*.
- Leder, A. & Geropp, D., 1993 Analysis of Unsteady Flows Past Bluff Bodies. *Journal of Wind Engineering and Industrial Aerodynamics* **49**, pp. 329-338.
- Lyn, D. A., Einav, S., Rodi, W., & Park, J.-H., 1995 A laser-Doppler velocimetry study of ensemble-averaged characteristics of the turbulent near wake of a square cylinder. *Journal of Fluid Mechanics* **304**, pp. 285-319.
- Magnus, G., 1852 On the Deflection of a Projectile. *Abhandlung der Akademie der Wissenschaftern Berlin*, (English translation in *Taylor's Scientific Memoirs*, 1853).
- Maskell, E. C., 1965 A Theory of the Blockage Effects on Bluff Bodies and Stalled Wings in a Closed Wind Tunnel. *Aeronautical Research Council, Reports and Memoranda* No. 3400 (supersedes some older ARC reports, 25 pp.).
- McNown, J. S. & Yih, C-S., 1953 Free-streamline analyses of transition flow and jet deflection. *Engineering Bulletin* **35**, State Univ. of Iowa.
- Milne-Thomson, L. M., 1968 *Theoretical Hydrodynamics*, 5th edition, Dover, NY.
- Mittal, S., 2003 Effect of a "slip" splitter plate on vortex shedding from a cylinder. *Physics of Fluids* **15**, pp. 817-820.

- Mittal, S. & Kumar, B., 2003 Flow past a rotating cylinder. *Journal of Fluid Mechanics* **476**, pp. 303-334.
- Morton, T. S., 1997 Application of an Elliptical Vortex Solution to a New Universal Strouhal Number and a Scalar Invariant for Drag Prediction., Ph.D. Dissertation, Brigham Young University, 1997.
- Najjar, F. M. & Balachandar, S., 1998 Low-frequency unsteadiness in the wake of a normal flat plate. *Journal of Fluid Mechanics* **370**, pp. 101-147.
- Okamoto, T., Yagita, M., & Ohtsuka, K., 1977 Experimental Investigations of the Wake of a Wedge. *Bulletin of the JSME* **20**, (141), pp. 323-328.
- Parkinson, G. V. & Jandali, T., 1970 A wake source model for bluff body potential flow. *Journal of Fluid Mechanics* **40**, pp. 577-594.
- Perry, A. E. & Steiner, T. R., 1987 Large-scale vortex structures in turbulent wakes behind bluff bodies. Part 1. Vortex formation processes. *Journal of Fluid Mechanics* **174**, pp. 233-270.
- Potts, J. R. & Crowther, W. J., 2002 FrisbeeTM Aerodynamics. *AIAA-2002-3150*, 15 pp.
- Protas, B. & Wesfreid, J. E., 2002 Drag force in the open-loop control of the cylinder wake in the laminar regime. *Physics of Fluids* **14**, pp. 810-826.
- Riabouchinsky, D., 1920 On steady fluid motions with free surfaces. *Proceedings of the London Mathematical Society* **19**, pp. 206-215.
- Roshko, A., 1954 A new hodograph for free streamline theory. *NACA Technical Note* 3168.
- Roshko, A., 1993 Perspectives on bluff body aerodynamics. *Journal of Wind Engineering and Industrial Aerodynamics* **49**, p. 79.
- Ruderich, R. & Fernholz, H. H., 1986 An experimental investigation of a turbulent shear flow with separation, reverse flow, and reattachment. *Journal of Fluid Mechanics* **163**, pp. 283-322.
- Sadovskii, V. S., 1971 Vortex Regions in a potential stream with a jump of Bernoulli's constant at the boundary. *Applied Mathematics and Mechanics* **35**, pp. 729-735.
- Schummy, D., 2005 *Guinness World Records 2006*, Guinness.
- Stojković, D., Breuer, M., & Durst, F., 2002 Effect of high rotation rates on the laminar flow around a circular cylinder. *Physics of Fluids* **14**, pp. 3160-3178.
- Stojković, D., Schön, P., Breuer, M., & Durst, F., 2003 On the new vortex shedding mode past a rotating circular cylinder. *Physics of Fluids* **15**, pp. 1257-1260.
- Swanson, W. M., 1961 The Magnus Effect: A Summary of Investigations to Date. *ASME Journal of Basic Engineering, D* **83**, pp. 461-470.
- Tanaka, H. & Nagano, S., 1972 Study of Flows about a Rotating Circular Cylinder. *Nippon Kikai Gakkai Ronbunshu* **38** (310), pp. 1343-1352.
- Thwaites, B., 1960 *Incompressible Aerodynamics*, Clarendon, Oxford.

- Tritton, D. J., 1959 Experiments on the flow past a circular cylinder at low Reynolds numbers. *Journal of Fluid Mechanics* **6**, pp. 547-567.
- Turfus, C., 1993 Prandtl-Batchelor flow past a flat plate at normal incidence in a channel - inviscid analysis. *Journal of Fluid Mechanics* **249**, pp. 59-72.
- Van Dyke, M., 1982 *An Album of Fluid Motion*, Parabolic Press, Stanford.
- Walsh, M.J. & Lindemann, A.M., 1984 Optimization and application of riblets for turbulent drag reduction, *AIAA Paper No. 84-0347*.
- Wieselsberger, C., 1922 Weitere Feststellungen über die Gesetze des Flüssigkeits- und Luftwiderstandes. *Physikalische Zeitschrift* **23**, pp. 219-224.
- Williamson, C. H. K., 1996a Three-dimensional wake transition. *Journal of Fluid Mechanics* **328**, pp. 345-407.
- Williamson, C. H. K., 1996b Vortex dynamics in the cylinder wake. *Annual Review of Fluid Mechanics* **28**, pp. 477-539.
- Wu, S. J., Miao, J. J., Hu, C. C., & Chou, J. H., 2005 On low-frequency modulations and three-dimensionality in vortex shedding behind a normal plate. *Journal of Fluid Mechanics* **526**, pp. 117-146.
- Wu, T. Y., 1962 A wake model for free-streamline flow theory Part 1. Fully and partially developed wake flows and cavity flows past an oblique flat plate. *Journal of Fluid Mechanics* **13**, pp. 161-181.
- Wu, T. Y., 1972 Cavity and wake flows. *Annual Review of Fluid Mechanics* **4**, pp. 243-284.
- Yang, J.-T., & Tsai, G.-L., 1992 The Wake Flow Structure of an Open-Slit V Gutter. *Experimental Thermal and Fluid Science* **5**, pp. 685-696.
- Yang, J.-T., Tsai, G.-L., & Wang, W.-B., 1994 Near-Wake Characteristics of Various V-Shaped Bluff Bodies. *Journal of Propulsion and Power* **10**, pp. 47-53.
- Yeung, W. W., H. & Parkinson, G. V., 1997 On the steady separated flow around an inclined flat plate. *Journal of Fluid Mechanics* **333**, pp. 403-413.

Appendix

In cases where the quantities necessary for calculating G in the mean recirculation region are reported directly from experimental studies, the following discussion is unnecessary. However, since these values are rarely available, the quantities must be deduced from available measurements in the wake.

In order to relate the time-mean wake vortex to the instantaneous vortex shedding, it is important to realize that the period, T_v , of the pair of elliptical vortices which constitute the time-mean recirculation region is related to the period, T_s , of the vortex shedding. In nominally planar flow, the period, T_v , of the time-mean elliptical vortex can be determined by integrating (10) around any elliptical streamline, as follows:

$$\int_0^{2\pi} d\bar{x}_2 = \int_0^{T_v} \frac{v_O}{a} dt \quad (27)$$

$$\therefore T_v = \frac{2\pi a}{v_O}. \quad (28)$$

With n vortices shed downstream per shedding cycle, we also have:

$$T_v = \frac{n}{f_s} \quad (29)$$

where f_s is the vortex shedding frequency. Eliminating T_v from (28) and (29) suggests the following potentially useful grouping:

$$S \equiv \frac{f_s a}{v_O} = \frac{n}{2\pi}. \quad (30)$$

For Reynolds numbers at which vortex shedding occurs, the frequency to be used in (30) is the vortex shedding frequency; below this Reynolds number range, it is the reciprocal of the period of the standing eddies. Solving (30) for v_O allows (19) to be written in terms of the shedding frequency rather than the vortex perimeter velocity ratio, as follows:

$$v_O = \frac{2\pi}{n} a f_s = \frac{2\pi a}{nD} St v_\infty$$

$$\therefore \frac{v_O}{v_\infty} = \frac{2\pi a}{nD} St \quad (31)$$

where St is the classical definition of the Strouhal number. The required velocity ratio in the time-average wake vortices can be determined by (31) unless a splitter plate trails the body, in which case the primary vortex shedding is eliminated.

Defining the Strouhal number in terms of the mean wake bubble allows a natural extension down to low Reynolds number flows exhibiting the pair of standing eddies. For Reynolds numbers at which vortex shedding occurs, the time-mean velocity field in the near wake still appears as a pair of counter-rotating, elliptical vortices (see, e.g., Van Dyke 1982). Below this Reynolds number range, the reciprocal of the period of the standing eddies can be used as the Strouhal frequency. As mentioned earlier, the quantity a is the maximum radius of the time-mean elliptical wake vortex, and v_O is the perimeter velocity at the minimum radius. The Strouhal number defined by (30) is equal to the characteristic vortex frequency divided by the real part of the vortex eigenvalue, $\lambda = \pm i v_O / a$, of the system $\dot{\mathbf{x}} = \mathbf{A} \mathbf{x}$. The near constancy of many Strouhal number groupings is due to the fact that they use length and velocity scales that are close to those of the eigenvalue of the mean wake vortex. The above relation allows the velocity field in the wake vortex to be estimated by measurements of the Strouhal number.